Applied Physics Letters ARTICLE scitation.org/journal/apl

Broadband acoustic absorbing metamaterial via deep learning approach

Cite as: Appl. Phys. Lett. **120**, 251701 (2022); doi: 10.1063/5.0097696
Submitted: 30 April 2022 · Accepted: 13 June 2022 ·
Published Online: 22 June 2022

Le Liu,[1,2,5] Long-Xiang Xie,[3,4] Weichun Huang,[1,5,6,a)] Xiu Juan Zhang,[1,5] Ming-Hui Lu,[1,4,5,6,a)] and Yan-Feng Chen[1,5]

AFFILIATIONS

[1]National Laboratory of Solid State Microstructures & Collaborative Innovation Center of Advanced Microstructures, Nanjing University, Nanjing 210093, China
[2]School of Physics, Nanjing University, Nanjing 210093, China
[3]School of Electronics and Information Engineering, Changshu Institute of Technology, Changshu 215506, China
[4]International Institute of Acoustic Technology, Suzhou 215513, China
[5]Department of Materials Science and Engineering, Nanjing University, Nanjing 210093, China
[6]Jiangsu Key Laboratory of Artificial Functional Materials, Nanjing University, Nanjing 210093, China

Note: This paper is part of the APL Special Collection on Acoustic and Elastic Metamaterials and Metasurfaces.
[a)]**Authors to whom correspondence should be addressed:** weichunhuang@nju.edu.cn and luminghui@nju.edu.cn

ABSTRACT

Sound absorption is important for room acoustics and remediation of noise. Acoustic metamaterials have recently emerged as one of the most promising platforms for sound absorption. However, the working bandwidth is severely limited because of the strong dispersion in the spectrum caused by local resonance. Utilizing the coupling effect among resonators can improve the absorbers' performance, but the requirement of collecting coupling effects among all resonators, not only the nearest-neighbor coupling, makes the system too complex to explore analytically. This Letter describes deep learning based acoustic metamaterials for achieving broadband sound absorption with no visible oscillation in a targeted frequency band. We numerically and experimentally achieve an average absorption coefficient larger than 97% within the ultra-broadband extending from 860 to 8000 Hz, proving the validity of the deep learning based acoustic metamaterials. The excellent ultra-broadband and near-perfect absorption performance allows the absorber for versatile applications in noise-control engineering and room acoustics. Our work also reveals the significance of modulating coupling effects among resonators, and the deep learning approach may blaze a trail in the design strategy of acoustic functional devices.

Sound absorption has been a long-standing topic in acoustics that has received much attention in science and engineering. Traditional sound absorbing materials are composed of microholes such as foams and fibers, which can be effectively regarded as homogeneous materials with energy dissipated during propagation. The absorption is weak within the low-frequency range because the dominant regime is the visco-inertial one, which is quite weak in this frequency band.[1]

During the past decade, acoustic metamaterials (AMs) based on the locally resonant mechanism have shown fascinating functionality in handling sound absorption with subwavelength units.[2,3] AMs are made up of artificial engineering structures that control, trap, and manipulate sound waves in ways that traditional materials cannot. AMs have given us a new, powerful platform for manipulating sound and vibrations, resulting in a variety of applications, such as negative refraction,[4,5] one-way transport,[6,7] acoustic imaging,[8,9] and perfect absorption.[10–13] In pursuit of perfect absorbers with subwavelength thicknesses, several AMs have been presented, including decorated membranes,[14,15] coiled Fabry–Pérot (FP) channels,[12,16,17] specialized Helmholtz resonators[18–20] in air, and bubble metascreens[21–23] in a water environment.

However, these structures featured local resonance, and the nature of strong dispersion largely limits the working bandwidth. Intuitively, one common and straightforward technique is combining several resonant components and piecing a broad absorbing band. Indeed, several broadband absorbers based on this technique are recently proposed by coupling multiple FP channels[17] or Helmholtz

resonators.[11,24] However, the antiresonances induced by the unexpected interplay among the local resonances cause rapid impedance oscillation and result in absorption dips. A fruitful strategy is cascading porous materials[25,26] or a microperforated panel,[27] which makes the system to become highly overdamped. Consequently, the absorption coefficient is nearly flat as a function of the frequency. Another strategy is based on the concept of a metaporous surface,[28,29] which embeds the resonant elements to enhance the density of states in a porous layer. An analytical model combining the modal decomposition and transfer matrix methods is used to achieve broadband absorption due to the low-quality factor resonances. Recently, nonlocal metamaterials and metasurfaces have been demonstrated to improve sound absorption performance[20,30] through modulating the mutual impedance from the coupling effect. However, the coupling effect in scattering problems is quite complex, because there is not only the nearest-neighbor coupling but also the long-range coupling effect. An analytical method is still a challenge especially when the coupling effect is multiple and strong enough.

Recently, deep learning has emerged as a promising computational tool that has been broadly applied. It contains multiple hidden layers to intelligently extract statistical rules and learn representations of big data. Therefore, deep learning is an excellent mathematical tool to find relationships in physical systems. Many works about combining deep learning with physics have been proposed, including optimization of photonic structures,[31] high-resolution imaging,[9,32] and acoustic object recognition.[33,34]

In this Letter, we investigate the coupling effect among FP channels and realize an absorber that shows near-perfect absorption (the average is larger than 0.97) in a broad frequency regime from 860 to 8000 Hz by harnessing the power of deep learning. The absorber is based on the causality constraint optimized metamaterials. Yet in discretized resonators' case, there are two methods to eliminate oscillations to approach the broadband absorption spectrum. One is increasing the effective dissipation.[25,27] Another route is increasing the mode density.[20] We adopt the second in this work. However, there are still some dips at the antiresonance points, which are induced by the evanescent waves. Taking a convolutional neural network to learn the feature of the evanescent waves will solve it. Finally, the almost perfect broadband sound absorption spectrum is obtained. The proposed network architecture consists of two cascade convolutional neural networks. The excellent broadband and near-perfect absorption performance allow the absorber for versatile applications in noise-control engineering and room acoustics.

The proposed absorber realizes near-perfect absorption starting at a low-frequency cutoff (900 Hz in this Letter), comprising 100 suitable FP channels arranged into a cuboid compactly, as sketched in Fig. 1(a). The geometric parameters H and W denote the length and width of the structure, t is the thickness of the walls, a is the side width, and l_n is the length of the nth channel. In the beginning, we make the length of channels obey the natural logarithm law to meet the designed mode distribution for the target absorption spectrum. The corresponding spectrum calculated through the numeric simulation is shown in Fig. 1(b), which has many dips at antiresonances since the coupling effect is too weak.[35] The FP channels are isolated partly so there are many peaks and dips.

Considering the coupling effect in FP channels, the renormalized impedance is given by[17]

$$Z_e^{-1} = \sum_{n=1}^{N} (Z_n)^{-1} + (\delta Z(\Lambda_{nn}, \Lambda_{nm}))^{-1}, \quad (1)$$

where Z_n is the surface impedance of the nth FP channel. In Eq. (1), the first term represents the bare response of the metamaterial, treating each FP channel to be independent from others and in parallel with each other as the local resonant element. It is irrelevant with coupling effects. The second term δZ represents the coupling effect. Λ_{nm} is from the coupling of different channels ($n \neq m$), Λ_{nn} represents the interaction within the same channels, acting like a self-energy term in

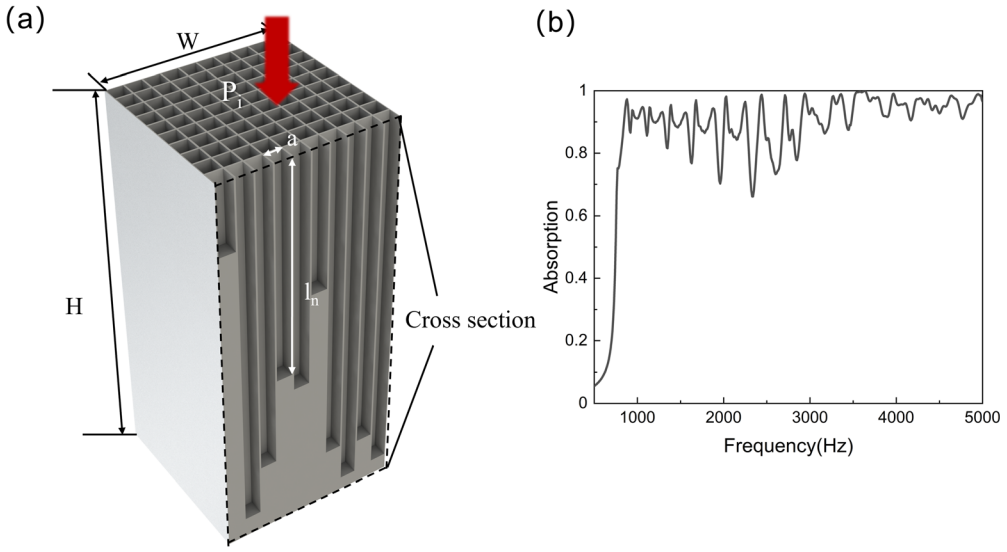

FIG. 1. (a) Schematic of 100 FP channels. The wall thickness is set as 0.5 mm, W = 50.5 mm and H = 110 mm are the width and length of the absorber, respectively, and the side width of the FP channel is 4.5 mm. (b) The calculated absorption spectrum of the left absorber.

a Dyson equation. Since Λ_{nn} is much larger than Λ_{nm}, previous studies ignore the influence of arrangement of resonators.[17,20]

However, in our structure, Λ_{nn} increases linearly with the number of channels N, and Λ_{nm} is nearly proportional to N^2. It is necessary to consider the coupling effect induced by arrangement when the number is large enough. To explore the influence caused by the arrangement of FP channels, we performed four sets of comparative structures in Fig. 2. The first structure was composed of two FP channels; as presented in Fig. 2(a), we change the arrangements in terms of the distance between two resonators, and there is no evident difference. The second term consists of 12 FP channels in Fig. 2(b), the same condition but accompanied by other ten resonators. There are evident differences at both 1400 and 2000 Hz. Compared with Fig. 2(a), the result tells us increasing the number of channels will strengthen the coupling effect. Moreover, we randomly rearrange the FP channels to evaluate the coupling effect among the different channels. The resulting absorption spectrum in Fig. 2(c) has only a small deviation after the rearrangement, verifying that the arrangement is not primary and can be ignored. However, in the last case (ten channels), the spectrum in Fig. 2(d) shows a marked difference after the rearrangement. It is a smoking-gun feature to the coupling effect induced by the orders of FP channels, and we can strengthen this coupling effect by increasing the number of FP channels, i.e., more intensive mode density.

Employing more resonators can lead to intensive mode density and strong coupling, which is demonstrated to suppress the antiresonances and broaden the bandwidth.[30,36] As demonstrated above, it is essential to account for the coupling effect induced by the arrangement. However, accumulating the whole coupling contribution among all resonators, including Λ_{nn} and Λ_{nm}, makes the system too complex to establish an analytical model.

In this situation, we apply optimization methods to modulate the coupling effect for a better broadband absorption spectrum. Traditional optimal approaches include evolutionary algorithms,[37] adjoint methods,[38,39] and genetic algorithms.[24] It often takes hundreds or even thousands of iterations to obtain a reasonable solution. Because simulation in our work is computationally expensive, these methods become prohibitively slow, especially with lots of iterations. To solve these challenges, we use a data-driven strategy based on deep learning technologies. Deep learning can find relationships in big data and accomplish the targeted goal without any iterative optimization.[40]

We introduce a deep learning model based on a two-dimensional convolutional neural network (CNN). Convolution operations take advantage of the spatial information and translational invariance, which make them more suitable to extract relevant features at a low computational cost compared to the fully connected neural networks. We propose an efficient modeling method that aims to establish the mapping between geometric parameters of metamaterial and the response sound absorption spectrum, as shown in Fig. 3.

First, we should establish a dataset to express the geometry structure parameters and corresponding absorption spectra. Introducing a structure matrix D which is composed of the length of channels, the channels' positions are labeled as $a_{1,1}, a_{1,2}, \ldots, a_{10,10}$. In a word, we encode the FP channels into a matrix D

$$D = \begin{bmatrix} a_{1,1} & \cdots & a_{1,10} \\ \vdots & \ddots & \vdots \\ a_{10,1} & \cdots & a_{10,10} \end{bmatrix}.$$

Meanwhile, the response absorption spectrum is encoded to a vector $R = (T_1, T_2, \ldots, T_{49})^T$, ranging from 400 to 5300 Hz, and the step is 100 Hz. The dataset about absorption spectra is conducted with the

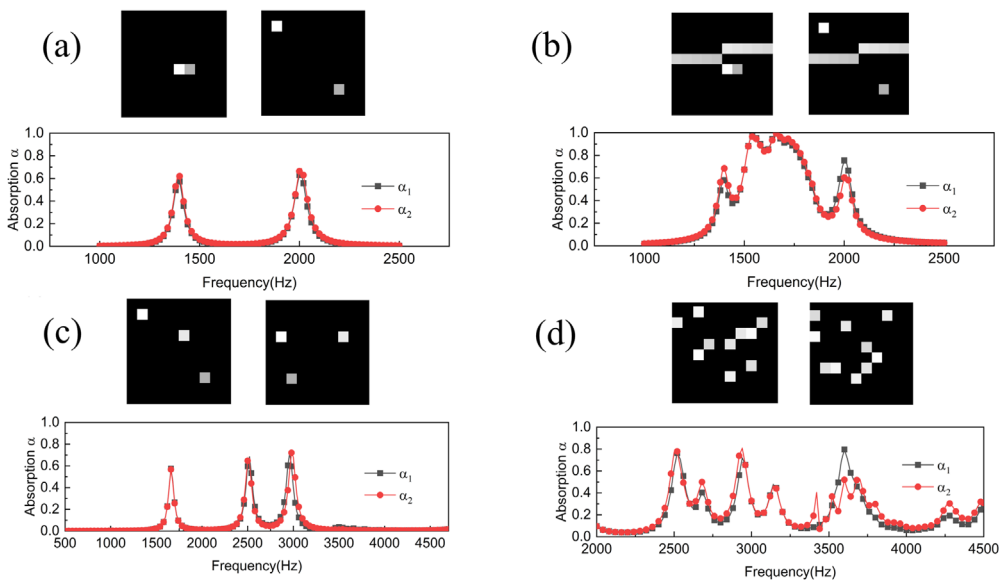

FIG. 2. (a) Different arrangement configurations comprised of two FP channels and the corresponding absorption spectra from simulation, the black curve for the first arrangement, and red for the second. The squares express FP channels, whose grayscale represents the length of channels. The whiter means the longer FP channel, and the black means the length is zero, i.e., no FP channel at this position. (b) The same configuration as (a) but accompanied by other ten FP channels. (c) Random distribution of three FP channels. (d) Random distribution of ten FP channels.

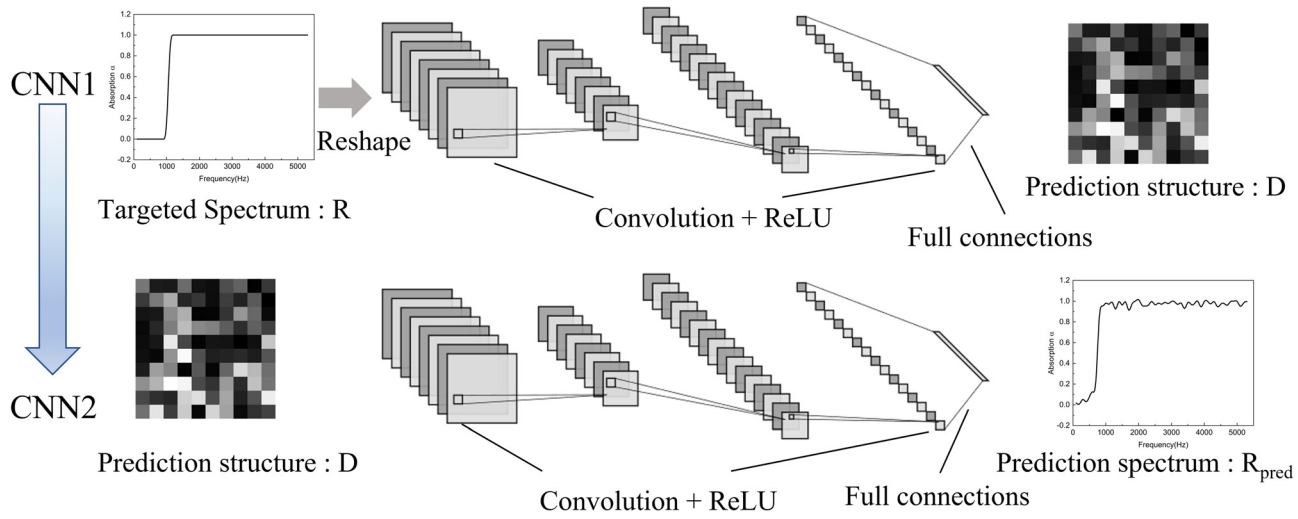

FIG. 3. Schematic diagram of the tandem network. The finite element method is used to calculate absorption spectra with different arrangements of 100 FP channels, randomly. CNN1 predicts the structure geometry parameters according to the target absorption spectra. CNN2 predicts the absorption spectra according to the structure geometry parameters. Cascading two CNN can solve the diverge issue caused by nonuniqueness in all inverse scattering problems.

preset pressure acoustics module of commercial software COMSOL Multiphysics. Sound hard boundaries are imposed on interfaces between air and solid due to the giant impedance mismatch. Stinson's model[41] is used to account for the viscous-thermal losses in FP channels, including the fundamental mode and higher-order mode. This type of model has a much lower computational cost compared to thermo-viscous acoustic models. Rearranging 20 000 pairs of structure matrices and the response absorption spectra randomly, we take 85% of the dataset as the training set and the rest 15% as the testing set. The configuration of our computer for data generations is AMD Ryzen^{TM} Threadripper^{TM} 2970X CPU@ 3.0 GHz/128GB/512G SSD. Now the data generation is finished.

Second, the CNN1 model is proposed to establish relationships from the response absorption spectrum set R to the structure matrix set D. The CNN1 model contains one input layer, four convolutional layers, one fully connected layer, and one output layer, as shown in Fig. 3. The input is the response absorption spectrum. To consider the 1D sequence as a 2D matrix, we reshape it from 1×49 to 7×7. The output is the structure geometry parameter. The number of feature maps of each convolutional layer is set as 64. The convolutional kernel size is chosen as 3×3. CNN1 is established to find the optimal structure geometry parameter for the targeted absorption spectrum.

Third, CNN2 is the second convolutional network to establish the relationship from structure geometry parameter set D to response absorption spectrum R. The CNN2 is the same as CNN1 except that the input layer and output layer are swapped. Rectified linear unit (ReLU) is the activation function in the two CNNs. For all training processes, the adapt moment estimation optimizer is chosen as the global optimizer. We chose batch-training methods, and the batch size is set to 128. The learning rate is 0.0001. To avoid discarding the same data every epoch, we set shuffling data before every epoch. Training is done by minimizing the loss function. We define loss and maximum error to evaluate the training effectiveness of CNNs. The loss is the average difference between the predicted absorption coefficient and simulated absorption coefficient. The maximum error is the maximum difference between the predicted absorption coefficient and simulated absorption coefficient. The loss is 0.036, and the maximum error is 0.065. The whole model training is achieved in Matlab R2021b. GTX 1080Ti GPU supports the training environment, and the total training time is about 10 min.

The convergent training of our network informs us that the deep-learning model can acquire the relationship between physical quantities. The target structures of our FP channels can be predicted quickly and intelligently. We randomly select several groups of absorption spectra that have different structures to verify the accuracy of this network. Parts of the predictions are shown in Figs. 4(a)–4(d). The data predicted (red curve with round) from our network match the simulated spectra from COMSOL Multiphysics (black curve with square) well. The predicted absorption spectra α_p and simulated spectra α_s overlap almost perfectly. The absolute value of the difference in absorption, defined as $|\alpha_p - \alpha_s|$, is plotted. The prediction of our network can fit well with the simulations when using various data, which indicates this network is robust.

Finally, after cascading CNN1 and CNN2, we can obtain an optimal absorption spectrum. It means that the deep learning optimized method is extraordinarily suitable for handling sound absorption. We set the targeted spectrum R near unity beyond the cutoff frequency; here, it is 900 Hz. Under the cutoff frequency, the absorption is zero. The predicted result R_{pred} is plotted in Fig. 5(c).

The experimental sample is fabricated by 3D-printing technology using the stereolithography apparatus with photosensitive resin. We use the lab-made impedance tube and measure the absorption coefficients through the two-microphone method,[42] as shown in Fig. 5(a). A photoimage of the impedance tube is presented in Fig. 5(b). Since the rear of the impedance tube is in the hard-wall condition, we assume that there is no transmission. The absorption spectrum can be obtained by analyzing the signal of microphones. The experimental, simulated, and network predicted absorption curves are plotted in

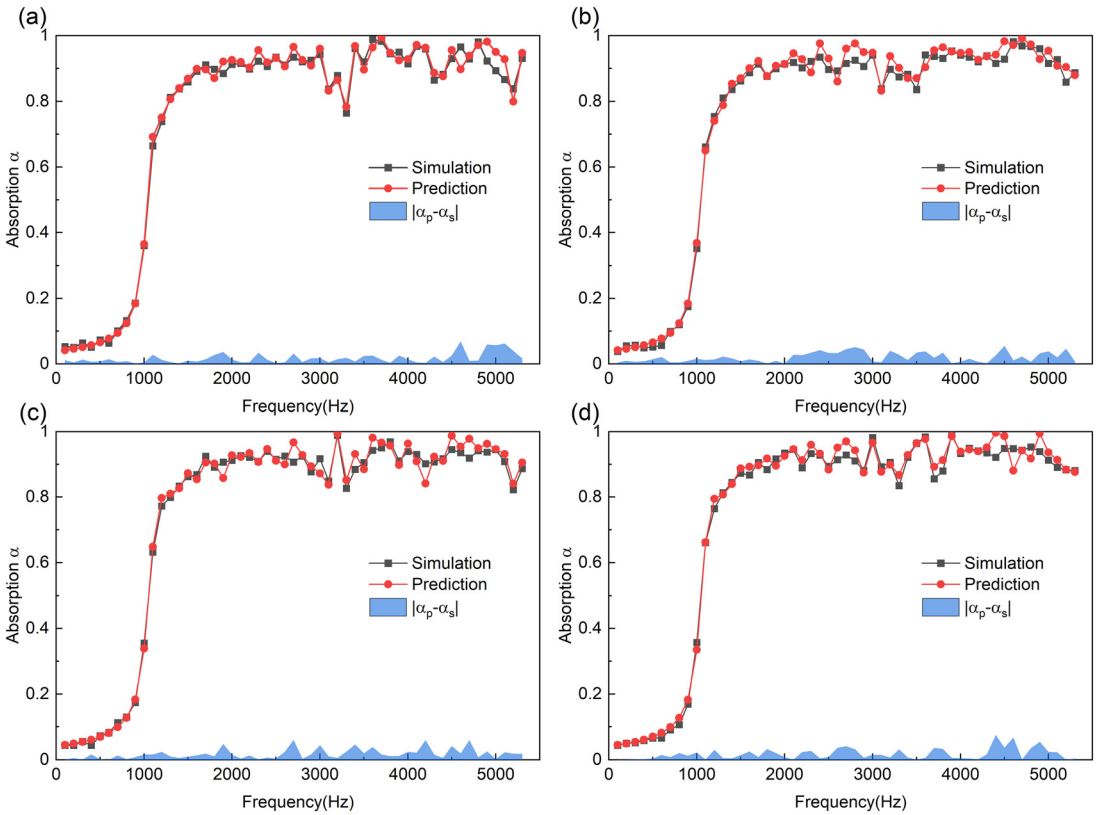

FIG. 4. (a)–(d) Instances of predicted absorption spectra through the network (red solid curves with round) and simulated spectra (black solid curve with square). The results demonstrate excellent accuracy in prediction with various input geometry parameters. The shade light blue area shows the absolute value of the difference in predicted and simulated absorption spectra, i.e., $|\alpha_p - \alpha_s|$.

Fig. 5(c). The simulated average absorption within the frequency of 860–3200 Hz is 98%, and the corresponding measured average absorption is 97.8%. Surprisingly, we find that the optimal absorber can achieve average absorption larger than 97% within 860–8000 Hz, and

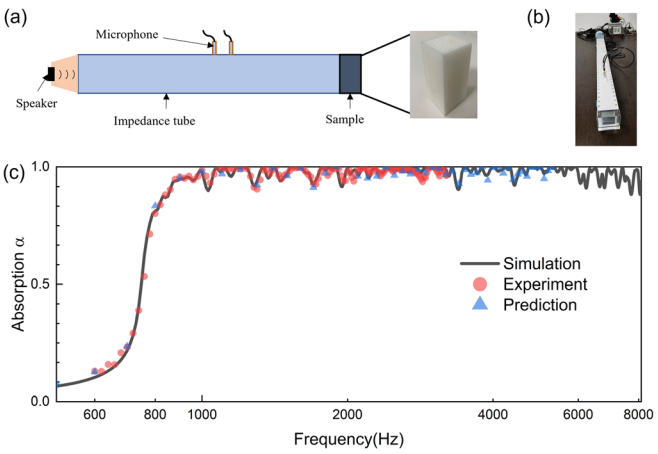

FIG. 5. (a) Schematic illustration of the 2D cross-sectional view of the experimental setup with an impedance tube and a photoimage of a sample. (b) A photo-image of the impedance tube. (c) Simulated, measured, and predicted absorption spectra.

the minimum value is 90.3% in numerical simulation. The experimental result is limited by the transfer-function method in impedance tubes. This method assumes only the plane wave mode propagates in tubes. To avoid the occurrence of nonplane wave mode propagation, the upper working frequency is set as $f_u < 0.5c_0/d$; here, c_0 is the speed of sound (343 m/s), and d is the side length of the rectangular tube, which is 50 mm. Therefore, the upper frequency we can test is around 3430 Hz. In our experimental results, the absorption spectrum ranges from 600 to 3200 Hz. The obtained results show excellent agreement, demonstrating the ultra-broadband sound absorption spectrum of the structure.

In conclusion, we investigate the influence of the coupling effect through rearranging the FP channels and experimentally realize an ultra-broadband absorption spectrum via a deep learning approach. In this method, CNNs are used to exploit the mapping between structure geometry parameters and response absorption spectra. The network predictions are validated by simulations and experiments. The average absorption is about 97% within the 860–8000 Hz frequency range. Coiling up the channels or designing other special compact geometry for the lower frequency response is the subsequent work. This artificial intelligence method can generate a certain mapping of other physical relationships, which are too complex, and the proposed methodology can be extended to other device designs on demand.

This work is supported by the National Key R&D Program of China (grant No.2021YFB3801800, No.2018YFA0306200, No. 2017YFA0303702), the National Natural Science Foundation of China (Grants No. 11890700, No.51732006, No.11625418).

AUTHOR DECLARATIONS

Conflict of Interest

The authors have no conflicts to disclose.

Author Contributions

Le Liu: Conceptualization (equal); Formal analysis (equal); Writing – original draft (equal); Writing – review and editing (equal). **Long-Xiang Xie:** Data curation (equal); Writing – original draft (supporting). **Weichun Huang:** Conceptualization (equal); Writing – original draft (equal). **Xiu Juan Zhang:** Formal analysis (supporting); Writing – original draft (equal). **Ming-Hui Lu:** Conceptualization (equal); Funding acquisition (equal); Supervision (equal); Writing – original draft (supporting); Writing – review and editing (supporting). **Yan-Feng Chen:** Supervision (equal); Writing – original draft (supporting).

DATA AVAILABILITY

The data that support the findings of this study are available from the corresponding authors upon reasonable request.

REFERENCES

[1]J. Allard and N. Atalla, *Propagation of Sound in Porous Media: Modelling Sound Absorbing Materials*, 2nd ed. (John Wiley & Sons, 2009).
[2]S. A. Cummer, J. Christensen, and A. Alù, Nat. Rev. Mater. **1**, 1 (2016).
[3]B. Assouar, B. Liang, Y. Wu, Y. Li, J.-C. Cheng, and Y. Jing, Nat. Rev. Mater. **3**, 460 (2018).
[4]M.-H. Lu, C. Zhang, L. Feng, J. Zhao, Y.-F. Chen, Y.-W. Mao, J. Zi, Y.-Y. Zhu, S.-N. Zhu, and N.-B. Ming, Nat. Mater. **6**, 744 (2007).
[5]Z. Liang and J. Li, Phys. Rev. Lett. **108**, 114301 (2012).
[6]B. Liang, X. S. Guo, J. Tu, D. Zhang, and J. C. Cheng, Nat. Mater. **9**, 989 (2010).
[7]R. Fleury, D. L. Sounas, C. F. Sieck, M. R. Haberman, and A. Alù, Science **343**, 516 (2014).
[8]J. Zhu, J. Christensen, J. Jung, L. Martin-Moreno, X. Yin, L. Fok, X. Zhang, and F. J. Garcia-Vidal, Nat. Phys. **7**, 52 (2011).
[9]B. Orazbayev and R. Fleury, Phys. Rev. X **10**, 031029 (2020).
[10]V. Romero-García, G. Theocharis, O. Richoux, and V. Pagneux, J. Acoust. Soc. Am. **139**, 3395 (2016).
[11]N. Jiménez, V. Romero-García, V. Pagneux, and J.-P. Groby, Sci. Rep. **7**, 13595 (2017).
[12]Y. Li and B. M. Assouar, Appl. Phys. Lett. **108**, 063502 (2016).
[13]M. Yang and P. Sheng, Annu. Rev. Mater. Res. **47**, 83 (2017).
[14]J. Mei, G. Ma, M. Yang, Z. Yang, W. Wen, and P. Sheng, Nat. Commun. **3**, 756 (2012).
[15]G. Ma, M. Yang, S. Xiao, Z. Yang, and P. Sheng, Nat. Mater. **13**, 873 (2014).
[16]X. Cai, Q. Guo, G. Hu, and J. Yang, Appl. Phys. Lett. **105**, 121901 (2014).
[17]M. Yang, S. Chen, C. Fu, and P. Sheng, Mater. Horiz. **4**, 673 (2017).
[18]H. Long, C. Shao, Y. Cheng, J. Tao, and X. Liu, Appl. Phys. Lett. **118**, 263502 (2021).
[19]H. Long, Y. Cheng, and X. Liu, Appl. Phys. Lett. **111**, 143502 (2017).
[20]Z. Zhou, S. Huang, D. Li, J. Zhu, and Y. Li, Natl. Sci. Rev. **2021**, nwab171.
[21]J. Mei, X. Zhang, and Y. Wu, J. Appl. Phys. **123**, 091710 (2018).
[22]M. Lanoy, R.-M. Guillermic, A. Strybulevych, and J. H. Page, Appl. Phys. Lett. **113**, 171907 (2018).
[23]V. Leroy, A. Strybulevych, M. Lanoy, F. Lemoult, A. Tourin, and J. H. Page, Phys. Rev. B **91**, 020301 (2015).
[24]V. Romero-García, G. Theocharis, O. Richoux, A. Merkel, V. Tournat, and V. Pagneux, Sci. Rep. **6**, 19519 (2016).
[25]M. Yang and P. Sheng, Appl. Sci. **8**, 1247 (2018).
[26]H. Long, C. Shao, C. Liu, Y. Cheng, and X. Liu, Appl. Phys. Lett. **115**, 103503 (2019).
[27]S. Huang, Z. Zhou, D. Li, T. Liu, X. Wang, J. Zhu, and Y. Li, Sci. Bull. **65**, 373 (2020).
[28]J. Boulvert, J. Costa-Baptista, T. Cavalieri, V. Romero-García, G. Gabard, E. R. Fotsing, A. Ross, M. Perna, J. Mardjono, and J.-P. Groby, Appl. Phys. Lett. **117**, 251902 (2020).
[29]J.-P. Groby, B. Brouard, O. Dazel, B. Nennig, and L. Kelders, J. Acoust. Soc. Am. **133**, 821 (2013).
[30]Y. Zhu, A. Merkel, K. Donda, S. Fan, L. Cao, and B. Assouar, Phys. Rev. B **103**, 064102 (2021).
[31]D. Liu, Y. Tan, E. Khoram, and Z. Yu, ACS Photonics **5**, 1365 (2018).
[32]T. Zhao, Y. Li, L. Zuo, and K. Zhang, Extreme Mech. Lett. **45**, 101297 (2021).
[33]J. Weng, Y. Ding, C. Hu, X.-F. Zhu, B. Liang, J. Yang, and J. Cheng, Nat. Commun. **11**, 6309 (2020).
[34]H. Wu, X. Wei, Y. Zha, and W. Jiang, J. Acoust. Soc. Am. **147**, 459 (2020).
[35]K. Y. Bliokh, Y. P. Bliokh, V. Freilikher, S. Savel'ev, and F. Nori, Rev. Mod. Phys. **80**, 1201 (2008).
[36]S. Huang, T. Liu, Z. Zhou, X. Wang, J. Zhu, and Y. Li, Phys. Rev. Appl. **14**, 021001 (2020).
[37]A. Gondarenko and M. Lipson, Opt. Express **16**, 17689 (2008).
[38]T. W. Hughes, M. Minkov, I. A. D. Williamson, and S. Fan, ACS Photonics **5**, 4781 (2018).
[39]A. Y. Piggott, J. Lu, K. G. Lagoudakis, J. Petykiewicz, T. M. Babinec, and J. Vučković, Nat. Photonics **9**, 374 (2015).
[40]A. Voulodimos, N. Doulamis, A. Doulamis, and E. Protopapadakis, Comput. Intell. Neurosci. **2018**, e7068349.
[41]M. R. Stinson, J. Acoust. Soc. Am. **89**, 550 (1991).
[42]ISO-10534-2, *Acoustics-Determination of Sound Absorption Coefficient and Impedance in Impedance Tubes-Part 2: Transfer-Function Method* (International Organization for Standardization, Geneva, Switzerland, 1998).